Star Formation in SpARCS J0330: Bridging the Gap Between Protoclusters and Clusters

J. Cairns[1], D. L. Clements[1], A. Noble[2], M. McDonald[3], Y. Ding[1], J. Nantais[4], G. Wilson[5]

[1]Imperial College London, Blackett Laboratory, Prince Consort Road, London, SW7 2AZ, UK • [2]ASU School of Earth and Space Exploration, 781 Terrace Mall, Tempe, AZ 85287, USA
[3]MIT Kavli Institute for Astrophysics and Space Research, Massachusetts Institute of Technology, 77 Massachusetts Avenue, Cambridge, MA 02139, USA
[4]Departamento de Ciencias Físicas, Universidad Andres Bello, Fernandez Concha 700, Las Condes 7591538, Santiago, Región Metropolitana, Chile • [5]Department of Physics and Astronomy, University of California, Riverside, CA 92521

1. Background

At **z > 2**, many studies have identified **protoclusters** - overdensities of galaxies spanning tens of Mpc in size and hosting some of the most vigorous star formation observed in the Universe to date. Conversely, **galaxy clusters** are typically observed at **z < 1** and are massive, virialised and abundant in quiescent, elliptical galaxies. Current models of galaxy formation and evolution predict that **protoclusters will evolve into z ~ 0 massive galaxy clusters** (e.g. Cooke et al. 2015), and so there must be some rapid, environmentally-driven quenching of star formation at $z \sim 1$ that transforms high-z, star-forming protoclusters into massive, quiescent galaxy clusters. However, **the exact nature of this evolution remains poorly understood**. In order to understand this evolution, **we must search for overdensities of galaxies at the onset of cluster formation** at which time we can observe the full web of activity: the assembly of a collapsed cluster core feeding on the star-forming filamentary material that resides in the protocluster web.

2. SpARCS J0330

We present observations of **SpARCS J0330, one of the most massive, high-z galaxy clusters ever discovered** (Lidman et al. 2012). SpARCS J0330 resides in the Chandra Deep Field South (CDFS) at a redshift of $z = 1.626$, with a dynamical mass of $\sim 2.5 \times 10^{14}\,M_\odot$. We combine the photometry and spectroscopy compiled by Nantais et al. (2016) with our own observations, as well as ancillary data in the field, to build up Spectral Energy Distributions (SEDs) for the 40 spectroscopically confirmed cluster members, as well as potential cluster members, with **up to 20-band photometry**. We use the photometric fitting codes `EAZY` (Brammer et al. 2008) and `CIGALE` (Boquien et al. 2019) to estimate the properties of these sources and hence **map out distant, star-forming galaxies over a ~ 15 Mpc region in the cluster**.

3. Sample Selection

1. **Spec-z sample**: Comprising the 40 spectroscopically confirmed cluster members. Available photometry includes *u*, *g*, *r*, *i*, *z*, *y*, *J*, *H* and *K* observations from IMACS, HAWK-I and HST, IRAC and MIPS photometry from *Spitzer* and PACS and SPIRE photometry from *Herschel*.
2. **Photo-z sample**: Sources with the same photometry as the spec-z sample but without a spectroscopically confirmed redshift.
3. **Photo-z wide sample**: Sources in the wider field from the Spitzer Data Fusion catalogue, including photometry from the HerMES, SWIRE, SERVS, VHS and VIDEO surveys, as well as CTIO MOSAIC2.
4. **Field sample**: We additionally assemble a field sample of sources from the Spitzer Data Fusion catalogue spread across the XMM-LSS field.

4. SED Fitting

We use the photometric fitting code `EAZY` to estimate photometric redshifts for the photo-z, photo-z wide and field samples, allowing us to select likely cluster candidates (see Figure 1). We then use `CIGALE` to estimate galaxy properties for all four samples. We use the `sfhdelayedbq` module to parameterise the star formation history according to:

$$\mathrm{SFR}(t) \propto \frac{t}{\tau^2} \times e^{-t/\tau} \text{ for } 0 \leq t \leq t_0$$

with the option of an instantaneous recent variation in SFR. We include a Chabrier IMF with solar metallicity and a dust attenuation curve based on that of Calzetti et al. (2000). We use the `nebular` emission module and the `Casey2012` dust module which models the FIR dust peak as a simple modified blackbody.

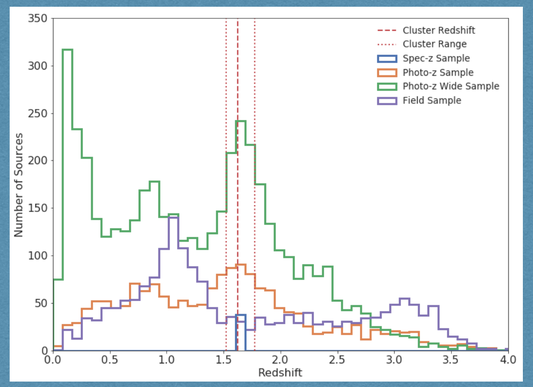

Figure 1 (*left*): Photometric redshift estimates from `EAZY` for our samples, as well as the spectroscopic redshifts for the spec-z sample. For our photo-z, photo-z wide and field samples we select cluster candidates and the corresponding field sample from one bin either side of the nominal cluster redshift (dashed red line) from Lidman et al. (2012).

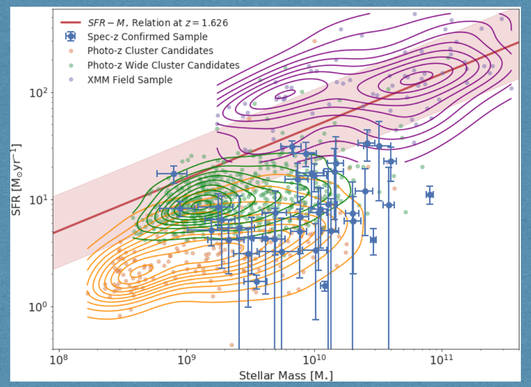

Figure 2 (*right*): The SFR - $M_\star$ relation for our four samples, alongside the relation for typical star-forming galaxies at $z = 1.626$ based on the parameterisation of Whitaker et al. (2012) with a scatter of 0.34 dex.

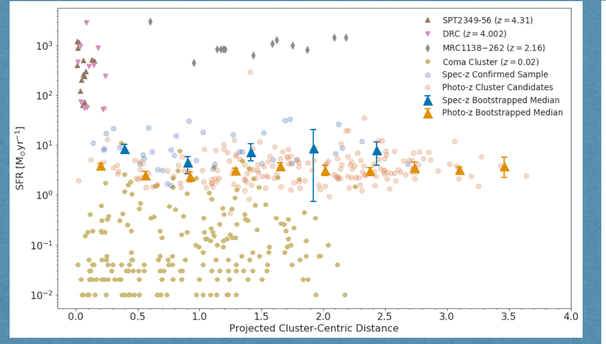

Figure 3 (*above*): SFR as a function of 2D projected cluster-centric radius for the individual sources in our spec-z and photo-z samples, as well as the bootstrapped median in bins of cluster-centric radius. For comparison we further show the DRC (Oteo et al. 2018) and SPT2349-56 (Miller et al. 2018) protoclusters at $z \sim 4$, the 'Spiderweb Cluster' (Dannerbauer et al. 2014) at $z \sim 2$ and the more local Coma Cluster (Edwards et al. 2011).

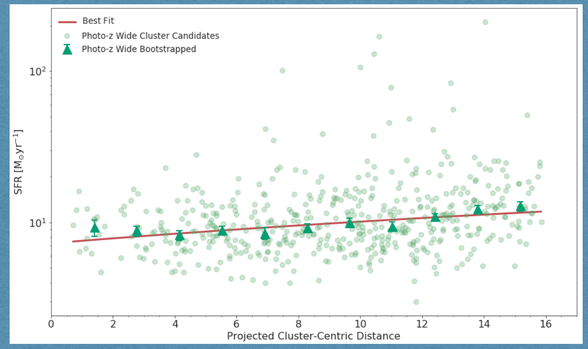

Figure 4 (*below*): SFR as a function of 2D projected cluster-centric radius for the individual sources in our photo-z wide sample, as well as the bootstrapped median in bins of cluster-centric radius. We fit a first order polynomial to the bootstrapped data, consistent with a gentle increase in SFR with cluster-centric radius in the wider field.

5. Results

In Figure 2 we present the SFR − $M_\star$ relation for all four of our samples, as well as the SFR − $M_\star$ relation for typical star-forming galaxies at $z = 1.626$. We find that **the majority of our sources lie below the main sequence.**

In Figure 3 we show SFR as a function of projected cluster-centric radius within the cluster core for our spec-z and photo-z samples, as well as estimating the bootstrapped median in bins of cluster-centric radius. We find that within the core of the cluster, **SFR remains flat as cluster-centric distance increases**, with median SFRs higher than Coma, but lower than the 'Spiderweb Cluster', the DRC and SPT2349-56. These results potentially indicate that **environmental quenching processes have already begun to influence the SFRs of the sources in the cluster core by z ~ 1.6**.

In Figure 4 we show the same SFR vs. cluster-centric radius plot for the wider field. We find that the results are consistent with a **gentle increase in SFR with cluster-centric distance**, potentially due to environmental quenching mechanisms (e.g. ram-pressure stripping, galaxy-galaxy interactions) truncating star formation as galaxies are accreted into the cluster.

In Figure 5 we show the spatial distribution of our spectroscopically confirmed cluster members overlaid on the density maps of the photo-z sample (*left*) and the photo-z wide sample (*right*). **We find some evidence of substructure**, with the photo-z sample displaying four density peaks within the cluster core following the distribution of the spec-z sources, and a further large density peak in the wider map to the North East.

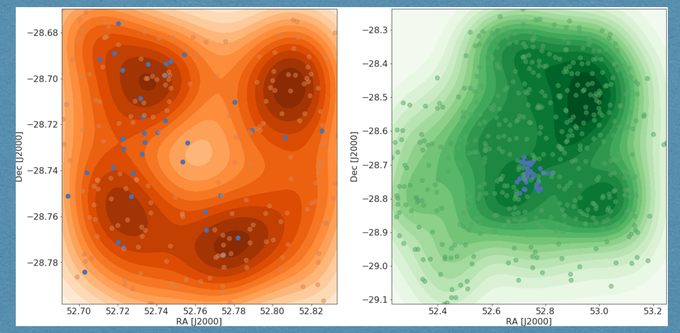

Figure 5: Spatial distribution of our spec-z sample (*blue points*) overlaid with the density map of our photo-z sample (*left - orange contours*) and our photo-z wide sample (*right - green contours*). We find that our spectroscopically confirmed cluster members are distributed across four density peaks in the photo-z sample. We also find evidence of substructure in the wider field, with another high density peak toward the North East.

6. Conclusions and Future Work

We have presented an analysis of the $z = 1.626$ cluster SpARCS J0330. By building up SEDs of up to 20-band photometry, we used the photometric fitting codes `EAZY` and `CIGALE` to estimate galaxy properties and map out star formation in the cluster.

- We find that SFR remains constant with projected cluster-centric distance within the core with median SFRs higher than the Coma Cluster but lower than in higher redshift clusters and protoclusters.
- In the wider cluster region, SFR increases gently with cluster-centric distance, likely due to the truncation of star-formation as galaxies are accreted into the cluster.
- The majority of the sources in the cluster reside below the SFR − $M_\star$ relation for typical star-forming galaxies at this redshift. These results potentially indicate that the environmentally-driven quenching of cluster galaxies has already begun between $z \sim 2$ and $z \sim 1.6$.
- The spatial distributions of our samples are potentially indicative of substructure within the cluster core and in the larger scale cluster region.

There is still plenty of exciting work to do for this project. Nantais et al. (2017) find that $z \sim 1.6$ clusters have low quenching efficiencies based on their optical/NIR photometry and Nantais et al. (2020) find that Hα-based SFRs for three $z \sim 1.6$ SpARCS clusters (including SpARCS J0330) are in agreement with field galaxies across a range of stellar masses. The disparity between these results and ours is likely due to the methods used for estimating SFR and the inclusion of additional FIR data, but this requires further investigation, including a comparison between our `CIGALE`-based SFRs and the Hα-based SFRs. We also plan to carry out observations focusing on spectroscopic confirmation of further cluster members from our photo-z and photo-z wide samples, as well as comparing these results to simulations of cluster formation and evolution such as ILLUSTRIS.

References: Boquien M., et al. 2019, A&A, 622, A103 • Brammer G., et al. 2008, ApJ, 686, 2 • Calzetti D., et al. 2000, ApJ, 533, 682 • Cooke E. A., et al. 2015, MNRAS, 452, 2318 • Dale, D. A., et al. 2014, ApJ, 784, 83 • Dannerbauer H., et al., 2014, A&A, 570, A55 • Edwards L. O. V., & Fadda D., 2011, AJ, 142, 148 • Lidman C., et al., 2012, MNRAS, 427, 550 • Miller T. B., et al., 2018, Nature, 556, 469 • Nantais J. B., et al., 2016, A&A, 592, A161 • Nantais J. B., et al., 2017, MNRAS, 465, 1 • Nantais J. B., et al., 2020, MNRAS, 499, 3 • Oteo I., et al., 2018, ApJ, 856, 72 • Whitaker K. E., et al. 2012, ApJ, 754, L29

Acknowledgements: The authors acknowledge funding support from the Royal Society as part of the International Exchanges Scheme.